

High-Capacity and Low-PAPR BICM-OFDM Systems Using Non-Equiprobable and Non-Uniform Constellation Shaping With Clipping and Filtering

Eito Kurihara, *Student Member, IEEE*, and Hideki Ochiai, *Fellow, IEEE*

Abstract—We address a design of high-capacity and low-peak-to-average power ratio (PAPR) orthogonal frequency-division multiplexing (OFDM) systems based on bit-interleaved coded modulation (BICM) utilizing non-equiprobable and non-uniform (NENU) constellations as well as clipping and filtering (CAF). The proposed constellations are generated using a truncated Gaussian distribution, and the merging of constellation points, where the former creates a non-uniform constellation (NUC), and the latter decreases the number of signal points without compromising the achievable bit-wise mutual information (BMI). Since the proposed constellations are uniquely determined by only the two parameters, each associated with NUC and cardinality, the complexity required for the numerical optimization process can be significantly low. We focus on the constellation design based on one dimension, i.e., pulse amplitude modulation (PAM), which facilitates the reduction of demapping complexity for the BICM receiver. The use of CAF at the transmitter can efficiently reduce the PAPR of OFDM signals; however, it introduces clipping noise that may degrade error rate performance, making the application of clipping noise cancellation (CNC) at the receiver essential. Therefore, we optimize the NENU constellations in the presence of CAF and CNC. Simulation results demonstrate that the combination of constellation shaping with CAF and CNC enables BICM-OFDM systems to simultaneously achieve low PAPR and high spectral efficiency over additive white Gaussian noise (AWGN) as well as frequency-selective Rayleigh fading channels. Furthermore, comparative studies confirm that the proposed system significantly outperforms the single-carrier counterpart (i.e., DFT-precoded BICM-OFDM) in terms of PAPR and bit error rate (BER) performance over fading channels.

I. INTRODUCTION

To achieve significantly high spectral efficiency under limited spectral resources, the use of quadrature amplitude modulation (QAM) with very large constellation sizes, together with capacity-approaching channel codes, is essential. A common practical approach is to combine bit-interleaved coded modulation (BICM) and the standard QAM, where the QAM is formed by two orthogonal Gray-labeled and equidistant (i.e., uniform) pulse amplitude modulation (PAM) symbols, each corresponding to in-phase (I) and quadrature (Q) channels. In this manner, coding and modulation can be performed in one-dimensional space. Furthermore, BICM allows us to decompose each space into parallel binary channels, where the conventional binary channel codes are applicable. This

structure significantly simplifies the complexity of demapping and decoding processes at the receiver [1].

The major drawback of BICM, especially with the standard Gray-labeled PAM symbols, is its achievable information rates that are inferior to the Shannon limit. The standard *uniform* PAM constellation, with each constellation point spaced equally from its neighbors, differs significantly from Gaussian signals that reach the Shannon limit. This discrepancy leads to a noticeable gap, especially when aiming for a higher target information rate. To reduce this gap, constellation shaping, which essentially controls the distribution of the PAM constellations to Gaussian, plays an important role.

Constellation shaping is classified as geometric and probabilistic shaping. Probabilistic shaping adjusts the probability distribution of the uniform PAM, whereas geometric shaping modifies the placement of constellation points [2,3]. Probabilistic shaping is typically implemented by introducing a distribution matcher, which entails high computational and storage complexity at the transmitter [4]. Geometric shaping is achieved by altering the locations of constellation points, making it compatible with current systems [5,6]. The design of a geometrically shaped constellation, often referred to as a nonuniform constellation (NUC), represents a significant area of ongoing research, particularly in conjunction with BICM [7–9].

In view of practical applications to systems with high spectral efficiency, we focus on the design for NUC of PAM (i.e., one-dimensional constellation) with a large constellation size. It is well known that the two-dimensional constellations can achieve higher performance in terms of the gap from the Shannon limit, but their implementation becomes challenging as the target information rate increases. In fact, existing wireless communication systems that aim for very high spectral efficiency employ modulation schemes based on one-dimensional constellations. For example, the Advanced Television Systems Committee’s third-generation standard (ATSC 3.0) adopts one-dimensional NUC (PAM) for higher-order cases such as 1024 and 4096 constellation points [10].

The major drawback of constellation shaping is that it increases peak-to-average power ratio (PAPR) as it attempts to reduce average power for a given maximum amplitude. It causes a significant reduction of power efficiency at the transmitter, as linear amplification of a high PAPR signal is challenging without sacrificing power amplifier efficiency [11]. This high PAPR issue is especially dominant with one-dimensional shaping, as the shape of the result-

E. Kurihara and H. Ochiai are with Graduate School of Engineering, The University of Osaka, Osaka, Japan. (email: kurihara-eito@ieee.org, ochiai@comm.eng.osaka-u.ac.jp)

ing two-dimensional constellation is rectangular rather than circular. Therefore, wireless systems that prioritize power amplifier efficiency, such as satellite communications, adopt circular constellations known as amplitude and phase shift keying (APSK), rather than rectangular constellations due to their lower PAPR. Nevertheless, other modern wireless communication systems adopt orthogonal frequency-division multiplexing (OFDM) for its higher spectral efficiency and robustness against fading channels, and since OFDM transmits multiple signals simultaneously, its PAPR turns out to be high regardless of the constellations used for each subcarrier, with or without shaping [12]. In such a framework, it is necessary to apply PAPR reduction techniques developed for OFDM signals, and they should have a high compatibility with constellation shaping.

A. Our Contributions

In this work, we design an OFDM system with *both* high spectral efficiency and low PAPR based on the combination of constellation shaping and clipping and filtering (CAF) [13]. Our constellation shaping is based on the use of one-dimensional NUC, where the number of constellation points is reduced from the original PAM consisting of signal points that are powers of two for reduced complexity without noticeable loss of performance. As a result, some constellation points are selected with higher probability than the others, leading to a non-equiprobable constellation. We refer to the resulting constellations as *non-equiprobable and non-uniform* (NENU) constellations.

Since CAF causes performance loss due to the in-band nonlinear distortion called clipping noise, we also consider the application of clipping noise cancellation (CNC) [14–16] such that the degradation is significantly mitigated at the receiver side. Overall, the system can achieve both low PAPR and high spectral efficiency, even within the practical framework of OFDM.

We summarize the main contributions of this work as follows:

- We propose a novel design algorithm for NENU PAM constellations, which combines a geometric design based on a truncated Gaussian distribution with a rate-adaptive constellation merging scheme¹. Numerical evaluations demonstrate that the proposed scheme achieves performance comparable to the numerically optimized NUC adopted in the ATSC standard.
- We design BICM-OFDM systems with low PAPR and high spectral efficiency, where low PAPR is achieved by CAF at the transmitter and high spectral efficiency is supported by CNC at the receiver that is compatible with our NENU constellations. We optimize the parameters associated with constellation shaping and PAPR reduction by analyzing bit-wise mutual information (BMI) in the context of CAF/CNC.

¹In [17], we first presented the concept of merging adjacent signal points for constellations designed according to truncated Gaussian distributions. The algorithm presented in this work is a refined version of [17] in that it can enhance the BMI through the merging process.

- Through computer simulations, we compare the proposed BICM-OFDM systems with the single-carrier counterpart [18] based on discrete Fourier transform (DFT) precoding that employs the same constellation shaping in terms of the complementary cumulative distribution function (CCDF) of PAPR, demonstrating that the proposed system with proper clipping ratio can achieve lower PAPR than the single-carrier systems in the presence of constellation shaping.
- Comparison of the resulting bit error rate (BER) performance over additive white Gaussian noise (AWGN) and frequency-selective Rayleigh fading channels shows that the proposed BICM-OFDM system provides noticeable gains in both channels. This is due to the CNC that successfully compensates for the BER degradation caused by CAF with no additional penalty in terms of receiver complexity associated with NENU constellations. It outperforms the single-carrier system with the same constellation over fading channels even with lower PAPR.

B. Related Work

Several systematic geometric shaping approaches based on Gaussian-like QAM constellations have been proposed in the literature [19–21] to enhance the achievable information rate while keeping design and implementation complexity modest. Despite their respective design variations, these methods share the common design principle of partitioning a Gaussian distribution into equiprobable sub-regions and assigning a representative constellation point to each sub-region, which was originally suggested in [22]. In our previous work [23], we proposed a systematic approach to designing non-uniform QAM constellations using a truncated Gaussian distribution adjusted by a single parameter. This method flexibly generates the constellation ranging from uniform to Gaussian-like distributions of [22], and we identify the parameter that maximizes the BMI under specified channel signal-to-noise ratios (SNRs). Nevertheless, the designed constellations fail to achieve the shaping gains as high as those of ATSC 3.0 [10], which are optimized based on an exhaustive numerical search. Moreover, the underlying design principles of such optimized NUCs remain largely unexplained, limiting theoretical understanding and systematic reproducibility.

As a low-complexity implementation of probabilistic shaping, a many-to-one mapping approach that does not rely on a distribution matcher can be employed [24–26]. In this method, redundant bit labels are introduced and they are assigned to a smaller number of constellation points such that the resulting probability mass function (PMF) approximates a Maxwell–Boltzmann (i.e., quantized Gaussian) distribution. Extensions to relatively high-order QAM constellations have recently been investigated in [27–29]. Since these approaches only require modifications to the bit-to-symbol mapping table, their implementation cost is significantly lower than those based on a distribution matcher. However, they tend to result in lower shaping gains due to their coarse approximation of the target distribution unless a considerably large number of shaping bits are used to adjust the PMF. Recent works [30–33] have also explored the integration of geometric and

probabilistic constellation shaping. Many of these approaches design the constellation geometry and symbol probabilities separately through numerical optimization.

In contrast, our approach offers a unified framework that jointly determines both the positions of constellation points and their probabilities based on a systematic design principle. Furthermore, the application of constellation shaping to OFDM systems with reduced PAPR has not been studied in the literature except for some earlier studies based on trellis shaping [34], which generally requires significant computation for PAPR reduction and causes rate loss for constellation shaping associated with the use of shaping bits.

C. Organization

The rest of this paper is organized as follows: Section II introduces our NENU constellation construction algorithm, followed by the performance analysis with parameter optimization in Section III. Section IV describes the proposed BICM-OFDM system model employing CAF and CNC, where the achievable information rate in this system model is analyzed. Simulation results are presented in Section V, focusing on the BER performance over practical fading channels and the CCDF of the resulting PAPR. Finally, Section VI concludes this work.

D. Notation

For a given scalar A_k , the corresponding bold font \mathbf{A} represents its row vector form. Sets of real positive numbers, complex numbers, and natural numbers are given by \mathbb{R}_+ , \mathbb{C} , and \mathbb{N} , respectively, whereas \mathbb{F}_2 represents the binary field; Calligraphy fonts such as \mathcal{A} represent sets, with their cardinality given by $|\mathcal{A}|$; $\mathcal{N}(\mu, \sigma^2)$ and $\mathcal{CN}(\mu, \sigma^2)$ represent real-valued Gaussian distribution and circularly symmetric complex Gaussian distribution, respectively, both having mean μ and variance σ^2 . Also, $\mathbb{E}[\cdot]$ denotes the expectation operation.

II. A NEW CONSTELLATION SHAPING ALGORITHM

In this section, we develop a novel systematic design for NENU PAM constellations by incorporating a constellation point merging strategy into the truncated Gaussian-based design. While the capacity of coded modulation (CM) systems increases with the number of distinct constellation points, this is not necessarily the case for BICM, as the optimal constellation cardinality that maximizes the BMI depends on the channel SNR. Therefore, we sequentially merge the adjacent Gaussian sub-regions into larger ones according to the target SNR. In other words, we partition a truncated Gaussian distribution into non-equiprobable sub-regions. We demonstrate that when the two design parameters (i.e., the number of distinct signal points and Gaussian truncation threshold) are jointly optimized, the resulting constellations closely match the numerically optimized NUCs without reducing the number of constellation points adopted in the standard. Unlike the latter, which requires a comprehensive table to specify the constellation points, a pair of parameters uniquely determines our constellation.

The proposed constellation design algorithm consists of two primary steps. We first formulate an initial constellation using a truncated Gaussian distribution and then merge the adjacent points. This algorithm thus facilitates a flexible constellation design in terms of the number of constellation points and their distribution, making it suitable for rate-adaptive designs in BICM systems.

A. Geometric Design Based on Truncated Gaussian CDF

We first review an M -ary PAM constellation design based on the truncated Gaussian distribution [23]. Due to the symmetry of constellation, it is sufficient to consider the constellation points within the positive region. Let $\mathcal{M}_+ \triangleq \{1, 2, \dots, M/2\}$ denote a set of constellation indices in this region. We define the set of corresponding constellation points as $\mathcal{A}_+ \triangleq \{a_k \in \mathbb{R}_+ \mid k \in \mathcal{M}_+\}$, with the elements ordered in the ascending order, i.e., $0 < a_1 \leq a_2 \leq \dots \leq a_{M/2}$. The constellation points are labeled by the binary reflected Gray code (BRGC), where the adjacent points differ only by a single bit. The most significant bit (MSB) is assigned as the sign bit such that a_k and $-a_k$ share the identical bit labels except for the MSB. Without loss of generality, we assume that MSB is 0 for the elements of \mathcal{A}_+ . The resulting constellation including the negative region is given by $\mathcal{A} = \mathcal{A}_+ \cup \mathcal{A}_-$, where $\mathcal{A}_- \triangleq \{-a_k \mid k \in \mathcal{M}_+\}$.

Since each PAM constellation point is selected with an equal probability, for a given target probability distribution, their locations are determined such that their cumulative distribution function (CDF) values are evenly distributed. Specifically, since the initial target distribution is Gaussian, we consider a random variable $X \sim \mathcal{N}(0, \frac{1}{2})$. The CDF of X is given by

$$F_X(x) = \frac{1 + \operatorname{erf}(x)}{2}, \quad (1)$$

where $\operatorname{erf}(x) = \frac{2}{\sqrt{\pi}} \int_0^x e^{-t^2} dt$ is the error function. Since the range of X is unbounded, we truncate its range within $[-b, b]$ for a given parameter $b > 0$. Accordingly, the range of the CDF in the positive region should be modified as $[\frac{1}{2}, F_X(b)]$. Thus, the tentative value \hat{a}_k , which corresponds to the point a_k before energy normalization, is determined by the following equality:

$$F_X(\hat{a}_k) = \frac{1}{2} + l_k \frac{F_X(b) - \frac{1}{2}}{M}, \quad (2)$$

where

$$l_k = 2k - 1, \quad \text{for } k \in \mathcal{M}_+ \quad (3)$$

is the integer value unique to the k th constellation point.

Let us define ρ as

$$\rho \triangleq \operatorname{erf}(b), \quad \rho \in (0, 1]. \quad (4)$$

We may then express \hat{a}_k in (2) using (1) as

$$\hat{a}_k = \phi_M(l_k; \rho) \triangleq \operatorname{erf}^{-1} \left(\rho \frac{l_k}{M} \right), \quad (5)$$

where $\phi_M : \mathbb{N} \rightarrow \mathbb{R}_+$ is a constellation mapper for a given parameter ρ .

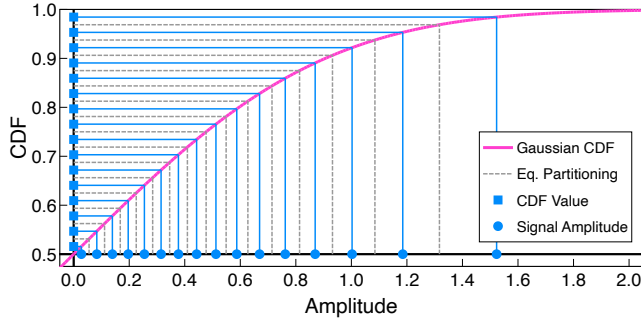


Fig. 1. Constellation point selection based on equiprobable partitioning of the Gaussian CDF ($\rho = 1$) with $M = 32$. Due to the symmetry, only the positive region is shown.

Finally, scaling the magnitude of \hat{a}_k in accordance with the energy constraint leads to the desired constellation point a_k :

$$a_k = \sqrt{\frac{E_s}{2}} \frac{\hat{a}_k}{\sqrt{\frac{2}{M} \sum_{k=1}^{M/2} \hat{a}_k^2}}, \quad (6)$$

where E_s is the energy in terms of QAM symbol.

This design algorithm uniquely determines the resulting constellation using a single parameter $\rho \in (0, 1]$ for a given modulation order M . When $\rho = 1$ (i.e., without truncation), the resulting constellation coincides with the Gaussian-like PAM proposed in [21]. In contrast, we may express the Maclaurin series of $F_X(x)$ up to the first order as

$$F_X(x) \approx \frac{1}{2} + \frac{1}{\sqrt{\pi}}x,$$

which indicates that $F_X(x)$ linearly increases (i.e., X becomes a uniform distribution) for $X \in [-b, b]$ in the limit of $b \rightarrow 0$ ($\rho \rightarrow 0$). For this reason, we denote $\rho = 0$ as the standard PAM in what follows.

The relationship between the CDF values and the selected constellation points $\{\hat{a}_k\}$ in the case of $M = 32$ and $\rho = 1$ (i.e., without range truncation) is illustrated in Fig. 1. As shown in the figure, the values $\phi_M(2(k-1); \rho)$ and $\phi_M(2k; \rho)$ serve as the boundary of the k th equiprobable sub-region, which are depicted as the corresponding gray dashed lines. Each sub-region is assigned a single bit label, and the representative constellation point \hat{a}_k is then selected to match the midpoint CDF value (i.e., $\phi_M(l_k; \rho)$) of its corresponding region.

B. Constellation Point Merging Process

Since the optimal constellation cardinality that maximizes the BMI varies depending on the channel SNR, we consider dynamically adjusting the number of constellation points by incorporating a constellation point merging strategy into the truncated Gaussian-based design described above.

We define N as the number of distinct points in M -ary PAM symbol with $N \leq M$, which means that a PAM constellation with M distinct labels has only N distinct constellation points. We denote this constellation as (M, N) -PAM in this work. The construction of (M, N) -PAM is given by the following recursive principle: adjacent point pairs in $\hat{\mathcal{A}}_+ \triangleq \{\hat{a}_k | k \in \mathcal{M}_+\}$

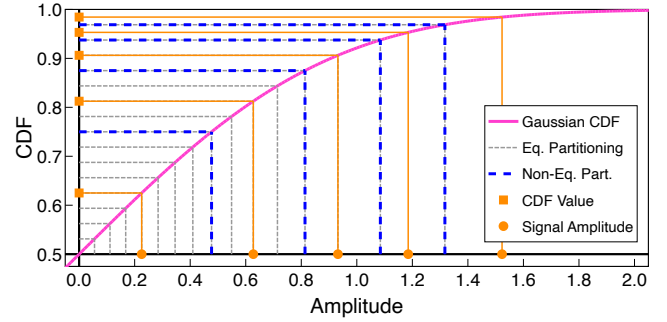


Fig. 2. Constellation point selection based on non-equiprobable partitioning of the Gaussian CDF ($\rho = 1$) with $M = 32$ and $N = 10$.

with the minimum Euclidean distance are merged sequentially until the number of distinct points reaches the specified size N . The merging of the two symmetrical pairs in the positive and negative regions occurs simultaneously, leading to a reduction of two constellation points at each merging step. Therefore, for an initial modulation order of M , the procedure can be executed a maximum of $M/2 - 1$ times in principle, ultimately leading to the standard BPSK constellation (when $N = 2$).

Each merging operation combines the corresponding sub-regions into a new, unified sub-region, and the representative constellation point is placed to match the midpoint CDF value of this modified sub-region. Now, suppose that for a given parameter ρ , the constellation points $\hat{a}_i = \phi_M(l_i; \rho)$ and $\hat{a}_j = \phi_M(l_j; \rho)$ (with $i \neq j$) have the minimum Euclidean distance at a certain merging step. Then, these two points are merged into a single point by updating their indices and amplitude values as²

$$\hat{a}_i = \hat{a}_j := \phi_M(l'; \rho), \quad l' := \frac{l_i + l_j}{2}. \quad (7)$$

After this process, the multiple bit labels originally associated with \hat{a}_i and \hat{a}_j are mapped to the identical signal amplitude. The proposed constellation shaping algorithm for a given pair of initial modulation order M and the number of distinct points N after the merging process is summarized in **Algorithm 1**, where \mathcal{L} corresponds to the set of the constellation indices in the positive region that have unique constellation point locations. The algorithm thus terminates when $|\mathcal{L}| = N/2$.

C. Example

The integer representations $\{l_k\}$ of the constellation points for the positive region $\hat{\mathcal{A}}_+$ obtained by **Algorithm 1** are listed in TABLE I in the case of $(32, N)$ -PAM starting from $N = 32$ to 2, where the initial constellation points are derived from the original Gaussian distribution (i.e., $\rho = 1$). The bit labels are based on BRGC. Therefore, the bit label of the negative region $-a_k$ is identical to that of a_k with MSB replaced by 1. Focusing on the first merging step from $N = 32$ to 30, the initial constellation points near the origin (e.g., $\hat{a}_1, \hat{a}_2, \hat{a}_3, \hat{a}_4$)

²Since the initial indices $\{l_k\}$ are set to be positive odd numbers according to (3), the first merging step always applies to the two positive odd numbers. As a result, the merged index l' is guaranteed to be a natural number.

TABLE I

The l_k INDICES OF CONSTELLATION POINTS $\hat{\mathcal{A}}_+$ FOR THE $(32, N)$ -PAM WITH $\rho = 1$ (NO TRUNCATION). THE SECOND ROW INDICATES THE BIT LABELS. THE INITIAL AMPLITUDE VALUES ARE SHOWN IN THE THIRD ROW, WHILE THE VALUES AFTER THE MERGING PROCESS ARE SHOWN IN BRACKETS. THE NUMBER IN THE LEFTMOST COLUMN REPRESENTS THAT OF DISTINCT POINTS N .

k	1	2	3	4	5	6	7	8	9	10	11	12	13	14	15	16	
bit label	00000	00001	00011	00010	00110	00111	00101	00100	01100	01101	01111	01110	01010	01011	01001	01000	
\hat{a}_k	.028	.083	.139	.196	.255	.315	.377	.443	.512	.587	.669	.762	.870	1.003	1.185	1.523	
32	1	3	5	7	9	11	13	15	17	19	21	23	25	27	29	31	
30	2 [.055]		5	7	9	11	13	15	17	19	21	23	25	27	29	31	
28	2		6 [.168]		9	11	13	15	17	19	21	23	25	27	29	31	
26	2		6		10 [.284]		13	15	17	19	21	23	25	27	29	31	
24	2		6		10			14 [.410]		17	19	21	23	25	27	29	31
22	2		6		10			14		18 [.549]		21	23	25	27	29	31
20	2		6		10			14		18		22 [.714]		25	27	29	31
18	4 [.111]			10			14			18		22		25	27	29	31
16	4			12 [.346]						18		22		25	27	29	31
14	4			12						18		22		26 [.932]		29	31
12	4			12						20 [.627]				26		29	31
10	8 [.225]				12				20				26		29	31	
8	8				12				20				26		30 [1.317]		
6	8				12				20				28 [1.085]				
4	8				12				20				24 [.813]				
2	16 [.477]																

Algorithm 1 Construction of (M, N) -PAM

Input: Modulation order M ; The number of distinct points N ; Shaping parameter $\rho \in (0, 1]$

Output: Constellation set $\hat{\mathcal{A}}_+$

- 1: $\mathcal{L} \leftarrow \{l_k := 2k - 1 \mid k = 1, 2, \dots, M/2\}$
- 2: $\hat{\mathcal{A}}_+ \leftarrow \{\hat{a}_k := \phi_M(l_k; \rho) \mid k = 1, 2, \dots, M/2\}$
- 3: **while** $M > N$ **do**
- 4: $(i, j) \leftarrow \arg \min_{(i,j)} |\hat{a}_i - \hat{a}_j|$ for $1 \leq i < j \leq M/2$
- 5: $\mathcal{L} \leftarrow \mathcal{L} \setminus \{l_i, l_j\}$
- 6: $\hat{\mathcal{A}}_+ \leftarrow \hat{\mathcal{A}}_+ \setminus \{\hat{a}_i, \hat{a}_j\}$
- 7: $l' \leftarrow \frac{l_i + l_j}{2}$
- 8: $\hat{a}_k \leftarrow \phi_M(l'; \rho)$
- 9: $\mathcal{L} \leftarrow \mathcal{L} \cup \{l'\}$
- 10: $\hat{\mathcal{A}}_+ \leftarrow \hat{\mathcal{A}}_+ \cup \{\hat{a}_k\}$
- 11: $M \leftarrow M - 2$
- 12: **end while**
- 13: **return** $\hat{\mathcal{A}}_+$

exhibit very small Euclidean distances. When the adjacent point pair \hat{a}_1 and \hat{a}_2 is merged, they are modified into a single signal point but with two distinct bit labels. Then, these merged symbols become indistinguishable from each other, but they become more separable from the remaining symbols (e.g., \hat{a}_3, \hat{a}_4). The conventional Gray labeling ensures that the interference from adjacent symbols results in only a single-bit error. However, in high-order constellations under low SNR conditions, the interference from non-adjacent symbols become likely as well, resulting in multiple-bit errors. The proposed constellation merging strategy effectively mitigates this issue by adaptively controlling the balance of density in terms of geometry and probability.

Fig. 2 illustrates the constellation point selection process based on the proposed merging scheme applied to the resulting constellation of Fig. 1, with the number of distinct points set

to $N = 10$. As shown in the figure, the original equiprobable sub-regions (gray dashed lines) are merged into larger sub-regions, depicted as blue dashed lines. Each representative constellation point is then selected in the same manner as that in Fig. 1, but based on the midpoint CDF value of the modified sub-region. This merging process corresponds to a non-equiprobable partitioning of the reference Gaussian distribution, according to the number of bit labels assigned to each constellation point.

We note that constellation point merging or many-to-one mapping in [26, 28, 29] refers to a low-complexity technique for implementing probabilistic shaping, where redundant bit labels are assigned to control the probability mass function (PMF) of the constellation to achieve shaping gain. In contrast, the proposed approach utilizes constellation point merging as an internal tool of geometric constellation design for the purpose of avoiding excessive density in the constellation. Therefore, this modification does not affect the complexity of the transmitter.

D. Comparison With NUC of ATSC 3.0

The proposed QAM constellation points consisting of two $(32, 20)$ -PAM constellations where the parameter ρ is optimized to maximize the BMI at the information rate corresponding to the code rate of $3/5$ (discussed in the next section) are depicted as green circles in Fig. 3. For comparison, those of the equivalent 1024-point NUC adopted in ATSC 3.0 are plotted as blue diamonds. While the ATSC NUC individually optimizes all 32 points per each dimension, many points around the origin are almost overlapping, resembling a smaller number of distinct points. Interestingly, the proposed constellation, systematically derived by **Algorithm 1** and governed by only the two design parameters N and ρ , exhibits a remarkably similar configuration to the NUC of ATSC 3.0. The performance analysis and optimization of these parameters

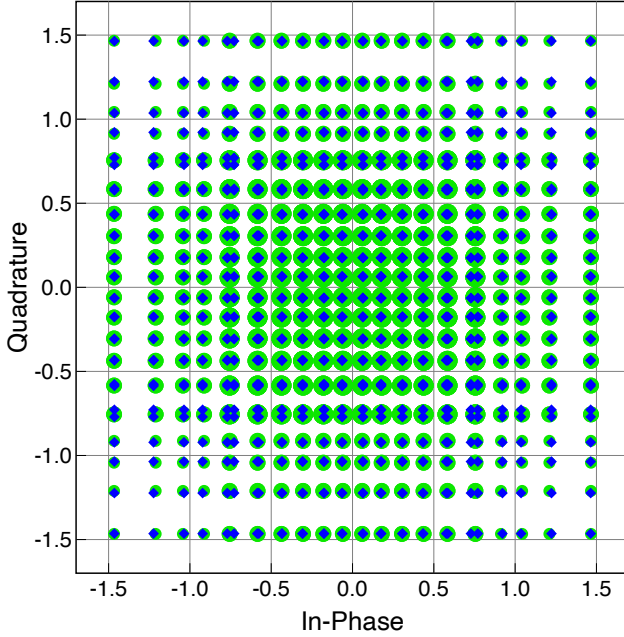


Fig. 3. Comparison between the proposed QAM consisting of two (32,20)-PAM constellations (shown as green circles) and the equivalent one-dimensional NUC adopted in ATSC 3.0 (shown as blue diamonds). Both constellations are optimized for BICM with an information rate of 8.333 bits per symbol (code rate of 3/5).

leading to the above result are presented in the following section.

III. PERFORMANCE ANALYSIS

This section analyzes the performance that can be achieved by the proposed constellation design through parameter optimization, focusing on achievable gain and demapping complexity. We compare the results with other constellations found through numerical optimizations, which require significantly higher complexity than the proposed scheme. From Section II-B, for a given modulation order M , the proposed constellation is specified by the two parameters, N and ρ . We denote the resulting constellation points located in both positive and negative regions by $\mathcal{A}(M, N, \rho)$ in what follows.

A. Total BMI

To identify the constellations that are expected to perform well, it is necessary to evaluate their achievable information rates. In BICM systems, the achievable information rate is defined by the BMI [1]. For a given M -ary PAM constellation \mathcal{A} , the total BMI at a specified channel SNR γ is given by

$$C(\mathcal{A}, \gamma) = n - \sum_{i=0}^{n-1} \mathbb{E}_{Y,b} \left[\log_2 \frac{\sum_{x \in \mathcal{A}} p_{Y|X}(Y|x)}{\sum_{x \in \mathcal{A}_b^{(i)}} p_{Y|X}(Y|x)} \right], \quad (8)$$

measured in bits per dimension, where $n = \log_2 M$ is the total number of binary channels and $\mathcal{A}_b^{(i)} \subset \mathcal{A}$ denotes the set of constellation points in the i th binary channel with the

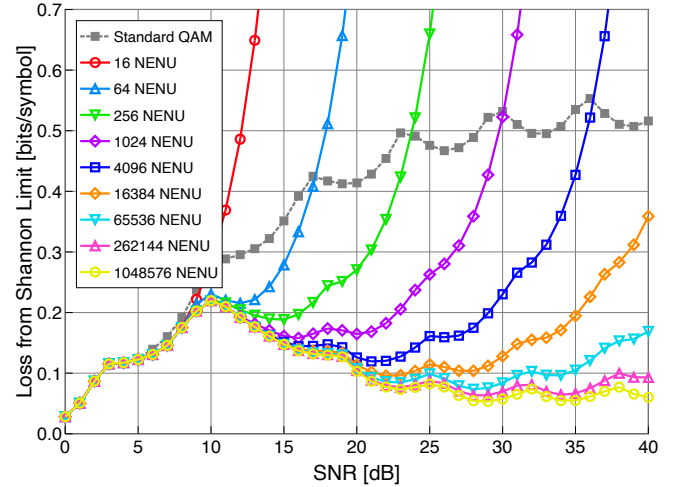


Fig. 4. Loss in achievable information rate from the Shannon limit for the BICM systems using the proposed constellations with various modulation orders.

bit specified by $b \in \mathbb{F}_2$. The conditional probability density function (PDF) $p_{Y|X}(y|x)$ is defined as

$$p_{Y|X}(y|x) = \frac{1}{\sqrt{\pi N_0}} e^{-\frac{(y-x)^2}{N_0}}, \quad (9)$$

where N_0 represents the power spectral density of AWGN, which is related to γ by $\gamma = E_s/N_0$.

B. Parameter Optimization

For a given pair of modulation order M and operating SNR γ , the optimization problem in our NENU constellation is formulated as

$$\begin{aligned} & \max_{N, \rho} C(\mathcal{A}(M, N, \rho), \gamma), \\ & \text{subject to } N \in \{2, 4, \dots, M\} \\ & \rho \in [0, 1]. \end{aligned} \quad (10)$$

By evaluating the BMI over all parameter pairs of (N, ρ) , the optimal constellation can be identified. (In practice, we may apply the quantized value of ρ with the step size of 0.01.) Note that when the channel is modeled as AWGN, the expectation over the Gaussian noise in the BMI calculation (8) can be efficiently computed using Gaussian–Hermite quadrature (GHQ) [35].

C. Loss From the Shannon Limit

The gain achieved by constellation shaping is typically assessed by the difference between the achievable information rate and the Shannon capacity, known as the *loss from the Shannon limit* [36]. When the two identical M -ary PAM constellations form M^2 -ary QAM, the loss from the Shannon limit is defined as a function of SNR γ by

$$L(\mathcal{A}, \gamma) \triangleq \log_2(1 + \gamma) - 2C(\mathcal{A}, \gamma) \quad (11)$$

in bits per symbol, where the second term corresponds to the total BMI of the two-dimensional QAM constellation.

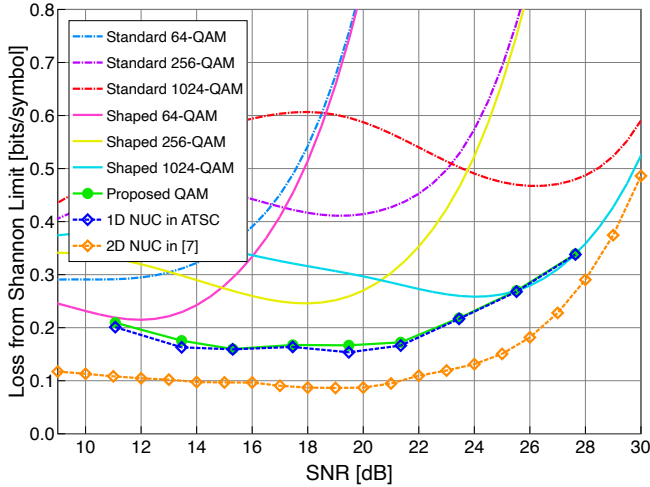


Fig. 5. Loss from the Shannon limit for the BICM systems with several different modulation schemes.

The loss from the Shannon limit of the proposed shaping scheme is shown in Fig. 4 for various modulation orders ranging from $M^2 = 16$ to $M^2 = 1048576$. Each plotted point is obtained by selecting the optimal parameter set (N, ρ) at a given SNR. As a comparison, the minimum loss achieved by the uniform M^2 -QAM with the optimized modulation order is indicated as a gray dashed line. At low SNRs, the performance of the proposed shaping scheme coincides with that of conventional QAM, due to the optimality of low-order constellations such as QPSK and uniform 16-QAM in this SNR regime. However, as the SNR increases, the gap between the BMI of standard QAM and the Shannon limit becomes noticeable. In contrast, the proposed NENU constellation consistently benefits from higher modulation orders across all SNRs. This indicates that, due to its flexible control over the number of signal points, properly designed NENU constellations successfully avoid excessive geometric density that would otherwise degrade the BMI. In fact, the proposed NENU constellation enhances the BMI because of an effect similar to probabilistic shaping.

D. Comparison With Other Geometric Shaping Schemes

We next compare the proposed NENU constellations with other constellations. For this purpose, we fix the modulation order as $M^2 = 1024$ in what follows. We consider the following numerically optimized constellations for comparison:

- The one-dimensional (1D) 1024-NUC of ATSC 3.0.
- The two-dimensional (2D) 1024-NUC developed in [7].
- The uniform M^2 -ary QAM with $M^2 \in \{64, 256, 1024\}$
- The one-dimensional shaping without constellation merging, i.e., $\mathcal{A}(M, M, \rho)$ with $M^2 \in \{64, 256, 1024\}$ (indicated as *shaped QAM*).
- The proposed one-dimensional NENU constellation $\mathcal{A}(32, N, \rho)$.

The results are compared in Fig. 5. We first observe that the optimal modulation order in BICM is contingent upon the channel SNR. The shaped QAM without constellation

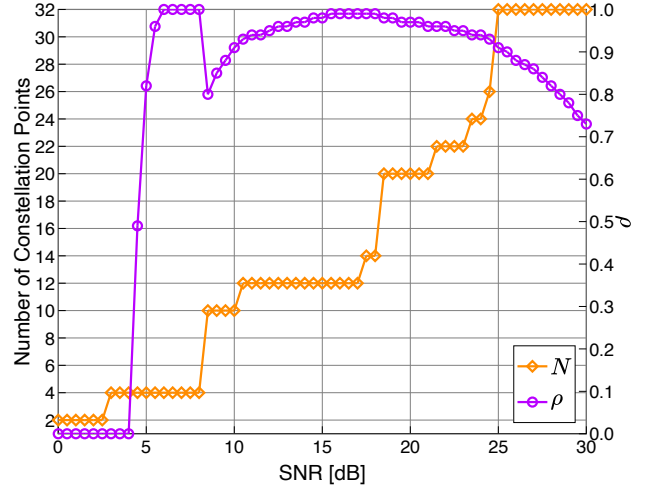


Fig. 6. The optimal values of constellation size N and design parameter ρ according to the channel SNR ($M = 32$).

merging has been confirmed to demonstrate improved performance compared to uniform QAM [23]. However, due to the constraint of constellation sizes to powers of two, these schemes exhibit significant gaps from the Shannon limit at specific SNR regions, particularly around 15 dB and 20 dB. In the case of the proposed shaping scheme, these gaps can be maintained at a minimal level across a wide range of SNR. This suggests that employing shaping with a flexible constellation size is advantageous for rate-adaptive BICM design. The gain achieved through the proposed shaping scheme is comparable to that of the one-dimensional NUC in ATSC 3.0 across all the SNRs, even though the latter is obtained by a more complex optimization process.

When comparing the results with the two-dimensional constellation of [7], performance gaps of approximately 0.08 bits per symbol are observed, highlighting the limitations inherent in one-dimensional constellation design. However, one-dimensional modulation schemes offer practical advantages in very high data-rate regimes, since the demapping process for two-dimensional constellations requires a considerable increase in computational cost with higher modulation orders, as is discussed in the next subsection.

E. Demapping Complexity

For efficient decoding, it is necessary to compute bit log-likelihood ratio (LLR) and this dominates the computational complexity at the receiver especially when irregular constellations are adopted. In what follows, we discuss the demapping complexity for general QAM constellations³.

Let us assume that the transmitted symbols are selected from a set of specific complex-valued (i.e., two-dimensional) constellation set \mathcal{A} , with the number of points represented by

³There have been several attempts to simplify the soft-output demappers for both one-dimensional and two-dimensional non-uniform constellations [37–40], but they rely on specific geometric structures of constellations.

$|\mathcal{A}|$. The LLR value for the i th bit level is computed as

$$L_i = \log \left[\frac{\sum_{x \in \mathcal{A}_0^{(i)}} \exp\left(-\frac{|y-x|^2}{N_0}\right)}{\sum_{x \in \mathcal{A}_1^{(i)}} \exp\left(-\frac{|y-x|^2}{N_0}\right)} \right] \approx \frac{1}{N_0} \left(\min_{x \in \mathcal{A}_1^{(i)}} \{|y-x|^2\} - \min_{x \in \mathcal{A}_0^{(i)}} \{|y-x|^2\} \right), \quad (12)$$

where $y \in \mathbb{C}$ denotes the received complex-valued symbol. We focus only on the number of required multiplication operations as the complexity associated with comparison and addition operations is considered negligible in comparison to that of multiplication operations.

On the other hand, if \mathcal{A} is a set of one-dimensional constellation points, the LLR value can be expressed as

$$L_i \approx \frac{1}{N_0} \left(\min_{x \in \mathcal{A}_1^{(i)}} \{(y-x)^2\} - \min_{x \in \mathcal{A}_0^{(i)}} \{(y-x)^2\} \right), \quad (13)$$

where $y \in \mathbb{R}$ is the received real-valued symbol and x is chosen from one-dimensional (i.e., real-valued) constellation.

In the case of a two-dimensional constellation, from (12) it is necessary to compute the squared Euclidean distances between the received symbol and each of the $|\mathcal{A}|$ constellation points. This computation entails performing $2|\mathcal{A}|$ real multiplications. Furthermore, the cardinality of the two-dimensional constellations is $|\mathcal{A}| = M^2$. On the other hand, in the case of a one-dimensional constellation, calculating (13) requires $|\mathcal{A}|$ real multiplications, and the corresponding cardinality is $|\mathcal{A}| = M$. Therefore, as M increases for higher spectral efficiency, the use of a one-dimensional constellation should be critical in view of practical implementation. This reasoning may elucidate the rationale behind the adoption of one-dimensional constellations for high-order scenarios in practical wireless communication systems such as ATSC 3.0, despite its lower achievable gain.

The proposed NENU constellation also offers a more efficient demapping implementation due to its reduced constellation size from M , since the demapping complexity is proportional to the actual number of constellation points N . With the modulation order set as $M = 32$, the optimal constellation size N and the design parameter ρ as a function of channel SNR γ are illustrated in Fig. 6. It is observed that the required number of distinct signal points decreases as the SNR decreases. It thus demonstrates that the proposed NENU constellation not only achieves near-optimal gain but also minimizes the demapping complexity.

IV. APPLICATION TO BICM-OFDM WITH CAF AND CNC

The design of wireless signals with low PAPR continues to be a prominent and challenging field of research [41–44], and a major practical drawback of constellation shaping is its increasing PAPR as it targets Gaussian distribution. On the other hand, BICM-OFDM is a *de facto* standard for high data rate wireless communications over frequency-selective fading channels, but due to its multicarrier nature, its signal has high PAPR regardless of the constellations employed. Thus, PAPR reduction should be necessary for better amplifier efficiency. Among many PAPR reduction approaches

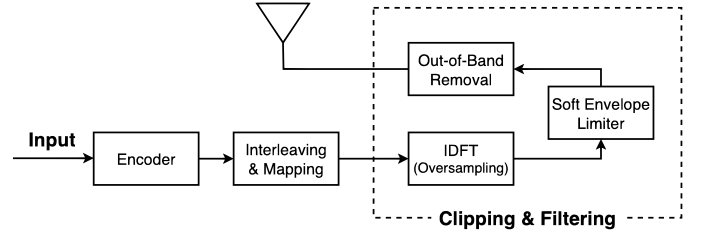


Fig. 7. Block diagram of the BICM-OFDM transmitter with CAF. CAF is implemented through a sequence of operations: oversampling using a JN_c -point IDFT, soft envelope limiter, and out-of-band signal removal.

developed for OFDM, we suggest employing CAF [13], as it is directly applicable to the standard OFDM systems. The major drawback is its nonlinear distortion, which should be compensated for at the receiver. Therefore, we also suggest using CNC [14], which allows us to take advantage of one-dimensional constellations for efficient implementation [15]. We demonstrate that the proposed NENU constellations can be flexibly optimized for such systems, achieving notable gains under practical scenarios.

In what follows, for simplicity of notation, we define the set of QAM symbols composed of the two NENU PAM constellations as

$$\mathcal{Z}_{M,N,\rho} \triangleq \{X_I + jX_Q \mid X_I, X_Q \in \mathcal{A}(M, N, \rho)\}.$$

A. OFDM Transmitter With CAF

We follow the description of [13] for CAF and that of [15] for CNC with an extension to coded OFDM. The block diagram of the OFDM transmitter with CAF is illustrated in Fig. 7. The information sequence is first encoded by a binary channel code with code rate $R_c \in (0, 1]$. The codeword is bit-wise interleaved and then mapped onto the corresponding NENU constellations. Let $\mathbf{Z} = (Z_0, Z_1, \dots, Z_{N_c-1}) \in \mathcal{Z}_{M,N,\rho}^{N_c}$ denote a vector of QAM symbols carried by each N_c -subcarrier OFDM signal, where $Z_k = X_{I,k} + jX_{Q,k}$ with $X_{I,k}$ and $X_{Q,k}$ representing NENU PAM symbol on the k th subcarrier. The J -times oversampled OFDM symbol $\mathbf{S} = (S_0, S_1, \dots, S_{JN_c-1}) \in \mathbb{C}^{JN_c}$ is generated by performing JN_c -point inverse discrete Fourier transform (IDFT) on the zero-padded symbol vector $\mathbf{Z}' = (\mathbf{Z}, \underbrace{0, 0, \dots, 0}_{(J-1)N_c}) \in \mathbb{C}^{JN_c}$ as

follows:⁴

$$S_n = \frac{1}{\sqrt{JN_c}} \sum_{k=0}^{JN_c-1} Z'_k e^{j2\pi k \frac{n}{JN_c}}, \quad n = 0, 1, \dots, JN_c - 1. \quad (14)$$

To restrict the peak power, these time domain signal samples are clipped by soft-envelope limiter [13] as

$$\tilde{S}_n = \begin{cases} S_n, & \text{for } |S_n| \leq A_{\max}, \\ A_{\max} e^{j \arg S_n}, & \text{for } |S_n| > A_{\max}, \end{cases} \quad (15)$$

⁴In practice, DFT and IDFT are implemented using the fast Fourier transform (FFT) algorithm by setting the number of points JN_c as the powers of two.

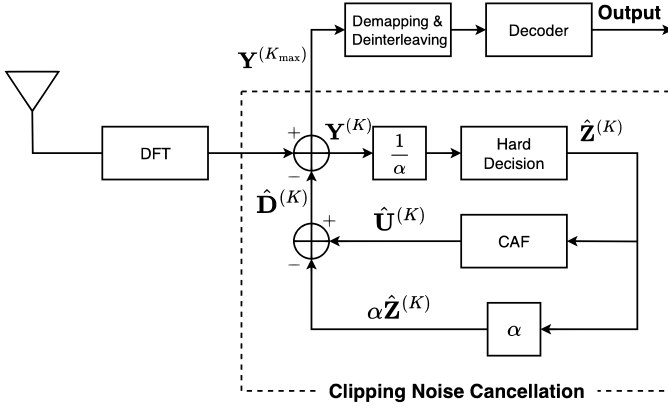


Fig. 8. Block diagram of the BICM-OFDM receiver with CNC. CNC iteratively estimates the clipping noise based on the regenerated clipped OFDM signal. Each iteration involves estimating the transmitted symbols and applying the CAF process, including JN_c -point IDFT and DFT.

where A_{\max} represents the maximum envelope level. We define the clipping ratio γ_{CR} as

$$\gamma_{\text{CR}} \triangleq \frac{A_{\max}}{\sqrt{P_{\text{in}}}}, \quad (16)$$

where $P_{\text{in}} \triangleq \mathbb{E}[\|\mathbf{Z}\|^2]/N_c$ is the average power of the OFDM signal prior to CAF. We then perform JN_c -point discrete Fourier transform (DFT) on the clipped signals to transform them back to the frequency-domain symbols represented by $\mathbf{U}' = (U'_0, U'_1, \dots, U'_{JN_c-1}) \in \mathbb{C}^{JN_c}$, where

$$U'_k = \frac{1}{\sqrt{JN_c}} \sum_{n=0}^{JN_c-1} \tilde{S}_n e^{-j2\pi k \frac{n}{JN_c}}, \quad k = 0, 1, \dots, JN_c - 1. \quad (17)$$

By removing the out-of-band component from these symbols, we obtain the in-band component $\mathbf{U} = (U_0, U_1, \dots, U_{N_c-1}) \in \mathbb{C}^{N_c}$ with $U_k \equiv U'_k$ as the transmit symbols.

The average power of the transmit OFDM signal after the CAF process is given by $P_{\text{av}} \triangleq \mathbb{E}[\|\mathbf{U}\|^2]/N_c$, i.e., the average signal power that includes the in-band distortion caused by clipping. For a fair comparison in terms of the transmit signal power and the channel noise variance, we define the SNR of an AWGN channel as

$$\text{SNR} \triangleq \frac{P_{\text{av}}}{N_0}. \quad (18)$$

The above definition of SNR ensures that the signal part is defined as the actual transmit signal including the in-band distortion (clipping noise).

B. OFDM Receiver With CNC

At the receiver, we consider performing CNC to mitigate the in-band distortion caused by CAF prior to channel decoding. The block diagram of the OFDM receiver with CNC is illustrated in Fig. 8. In the case of an AWGN channel, the received symbol corresponding to the k th subcarrier can be expressed as

$$\tilde{Z}_k = \alpha Z_k + D_k + W_k, \quad (19)$$

where $D_k \in \mathbb{C}$ denotes the distortion component caused by the CAF process and $W_k \in \mathbb{C}$ represents the Gaussian noise with

$W_k \sim \mathcal{CN}(0, N_0)$, both corresponding to the k th subcarrier. Assuming that the baseband OFDM signal follows a complex Gaussian distribution, the attenuation factor α due to clipping can be expressed as [13]

$$\alpha = 1 - e^{-\gamma_{\text{CR}}^2} + \frac{\sqrt{\pi}\gamma_{\text{CR}}}{2} \text{erfc}(\gamma_{\text{CR}}), \quad (20)$$

where $\text{erfc}(x) = 1 - \text{erf}(x)$. Provided that the length of cyclic prefix is sufficient compared to that of the channel impulse response, the received symbol over a frequency-selective fading channel can be expressed as

$$Y_k = H_k (\alpha Z_k + D_k) + W_k, \quad (21)$$

where H_k is the channel coefficient of the k th subcarrier. Assuming that the channel coefficients can be perfectly estimated at the receiver, we may apply the zero-forcing (ZF) equalization as

$$\tilde{Y}_k \triangleq \frac{Y_k}{H_k} = \alpha Z_k + D_k + W'_k, \quad (22)$$

where $W'_k \triangleq W_k/H_k \sim \mathcal{CN}(0, N_0/|H_k|^2)$.

In the CNC process, we iteratively estimate and remove the distortion component $\mathbf{D} = (D_0, D_1, \dots, D_{N_c-1}) \in \mathbb{C}^{N_c}$. The CNC algorithm at the K th iteration (starting with $K := 0$) is described as follows:

- 1) Apply the hard decision based on the constellation set $\mathcal{A}(M, N, \rho)$ to the equalized and normalized received signal $Y_k^{(K)}/\alpha$ (with $Y_k^{(0)} := \tilde{Y}_k$) to estimate the transmitted symbol $\hat{Z}_k^{(K)} = \hat{X}_{I,k}^{(K)} + j\hat{X}_{Q,k}^{(K)}$, which is given by

$$\begin{cases} \hat{X}_{I,k}^{(K)} = \arg \min_{X \in \mathcal{A}(M, N, \rho)} \left(X - \Re \{ Y_k^{(K)} \} / \alpha \right)^2, \\ \hat{X}_{Q,k}^{(K)} = \arg \min_{X \in \mathcal{A}(M, N, \rho)} \left(X - \Im \{ Y_k^{(K)} \} / \alpha \right)^2. \end{cases} \quad (23)$$

- 2) Apply the same CAF process at the transmitter to obtain the estimated in-band component, which can be modeled as

$$\hat{U}_k^{(K)} = \alpha \hat{Z}_k^{(K)} + \hat{D}_k^{(K)}. \quad (24)$$

- 3) Calculate the distortion component by

$$\hat{D}_k^{(K)} = \hat{U}_k^{(K)} - \alpha \hat{Z}_k^{(K)}, \quad (25)$$

and subtract it from the original received symbol as

$$\begin{aligned} Y_k^{(K+1)} &= \tilde{Y}_k - \hat{D}_k^{(K)} \\ &= \alpha Z_k + \left(D_k - \hat{D}_k^{(K)} \right) + W_k. \end{aligned} \quad (26)$$

- 4) Set $K := K + 1$. If K reaches the iteration limit K_{\max} , output $Y_k^{(K_{\max})}$ and stop. Otherwise, go to Step 1).

Note that each iteration involves CAF at the receiver side, which requires performing JN_c -point IDFT, clipping, and JN_c -point DFT at Step 2).

If the majority of the estimated symbols are correct, the residual distortion component $D_k - \hat{D}_k^{(K)}$ should diminish as K increases. This cancellation process may be successful when the channel SNR is sufficiently high. Since our target

is a high spectral efficiency regime, this high-SNR assumption naturally applies, and thus CNC is expected to work properly, provided that the clipping ratio γ_{CR} is appropriately selected. Although a lower clipping ratio helps reduce PAPR and improve power amplifier efficiency, it introduces more severe nonlinear distortion, which may prevent CNC from functioning properly.

Note that since our NENU constellations are designed based on a one-dimensional constellation, the complexity associated with the hard decision in (23) is significantly lower than that of the two-dimensional constellation, similar to the argument of demapper complexity. This observation also justifies the use of one-dimensional constellations for our BICM-OFDM systems involving CAF and CNC⁵.

C. Parameter Optimization for OFDM with CAF and CNC

1) *System Setup*: In the following numerical results, we consider the specific system where the number of subcarriers is $N_c = 1024$ and each subcarrier is modulated by 32-PAM per dimension (1024-QAM per subcarrier symbol) with $R_c = 5/6$. The resulting spectral efficiency is 4.166 bits per dimension, or 8.333 bits per complex channel use. Based on the preliminary analysis, the clipping ratio of $\gamma_{CR} = 1.5$ is found to be the minimum acceptable value that does not impose malfunctioning of CNC operation⁶. Although some residual clipping noise still remains as a result of CNC, the proposed system can be designed to operate properly with $\gamma_{CR} = 1.5$. Both AWGN and fading channels are considered, where in the case of fading channels we adopt frequency-selective Rayleigh fading channel with an uncorrelated four-path equal-power delay profile as a specific example. The proposed NENU constellation used in each system is optimized based on the corresponding channel condition.

2) *Parameter Optimization*: We optimize the system based on (10), where the BMI is computed using (8) by observing the received symbol that serves as an input to the channel decoder. Note that for the systems employing CAF and CNC, the channel becomes a mixture of AWGN and residual clipping noise, which may not be described by a tractable mathematical model. Therefore, we compute the resulting BMI based on simulations, making the optimization process more computationally intensive compared to the AWGN channels without CAF.

We consider the following three cases:

- A. Without CAF, both AWGN and fading channels
- B. With CAF and CNC, AWGN channel
- C. With CAF and CNC, fading channel

For each case, the following optimal parameter sets are found through preliminary simulations:

⁵It is possible to design CNC that takes into account the channel decoder output as well as re-encoder in its loop, but this approach makes not only the receiver complexity and latency prohibitive, but also the appropriate system design more challenging.

⁶Optimal clipping ratio may be mathematically analyzed in terms of signal-to-noise plus distortion power ratio (SNDR) when CAF is applied [45], but since our system makes use of CNC at the receiver, its error rate performance depends on several parameters such as the number of subcarriers and constellations [15]. Therefore, it may be mathematically intractable.

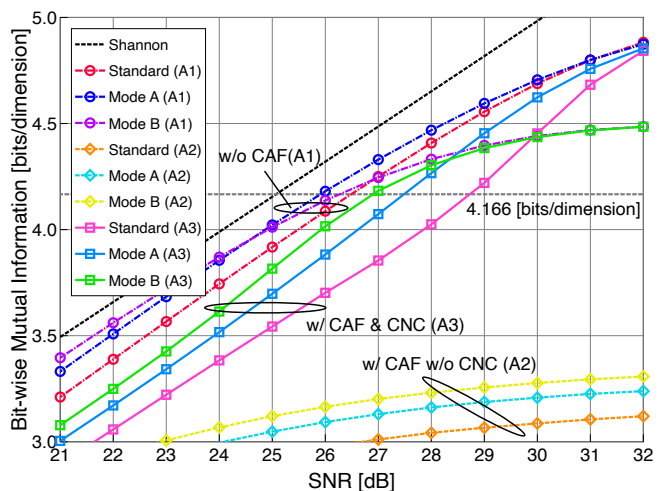


Fig. 9. Comparison of BMI values for 32-PAM constellations over an AWGN channel. The following three systems are evaluated: A1) Without CAF, A2) with CAF only, and A3) with CAF/CNC. (Parameters: $\gamma_{CR} = 1.5$ for CAF and $K_{max} = 10$ for CNC.)

- A. $N = 32$, $\rho = 0.88$ (SNR = 26 dB)
- B. $N = 24$, $\rho = 0.93$ (SNR = 27 dB)
- C. $N = 28$, $\rho = 0.97$ (SNR = 33 dB)

In what follows, we refer to the NENU constellations designed by the above parameter sets as Modes A, B, and C, respectively.

From the above results, we observe that the optimal number of constellation points depends on the channel conditions, which agrees with the trend discussed in Section III. Without CAF, $N = 32$ is selected as optimal due to the high spectral efficiency assumption with $R_c = 5/6$. In contrast, with CAF and CNC, smaller values of N are preferred to better accommodate the residual nonlinear distortion that reduces the effective SNR.

We note that constellation design based on exhaustive numerical optimization algorithms, such as particle swarm optimization (PSO), does not rely on a predefined set of constellation candidates. Consequently, optimizing the objective functions such as the BMI after CAF and CNC processing becomes computationally demanding. On the other hand, the proposed design requires evaluation over a limited number of constellation candidates determined only by the two parameters. It thus reduces the computational burden significantly and enables optimization in an efficient manner, even under such complicated system constraints.

3) *Total BMI*: We evaluate the total BMI over an AWGN channel for the following three systems:

- A1**: BICM-OFDM without CAF (no PAPR reduction)
- A2**: BICM-OFDM with CAF but without CNC
- A3**: BICM-OFDM with CAF and CNC.

The results are compared in Fig. 9, where the parameters of the NENU constellations are fixed as either Mode A or B over the entire channel SNR. The uniform PAM is also shown as a reference. In **A1**, Mode A demonstrates superior performance compared to the others at the target information rate. On the other hand, in **A2**, the achievable rates of all constellations significantly deviate from the target as a result

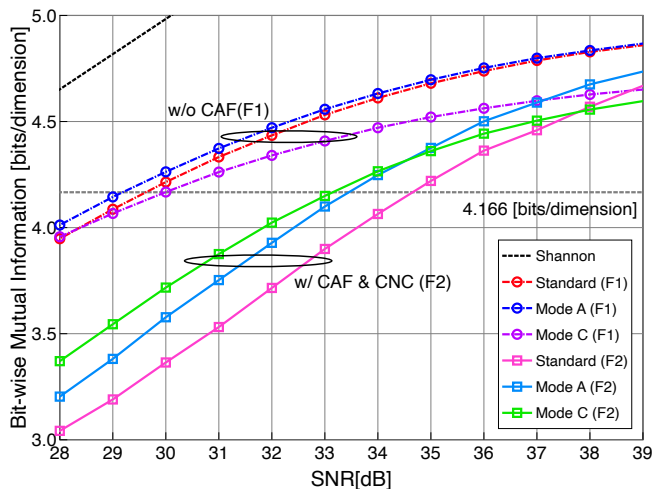


Fig. 10. Comparison of BMI values for 32-PAM constellations over a frequency-selective Rayleigh fading channel. The following two systems are evaluated: F1) Without CAF and F2) with CAF and CNC. (Parameters: $\gamma_{CR} = 1.5$ for CAF and $K_{max} = 10$ for CNC.)

of severe clipping noise. Finally, in **A3**, the information rate is successfully recovered by CNC, allowing the target information rate to be achieved with a lower PAPR compared to **A1**. Mode B demonstrates superior performance, yielding a greater gain over Mode A. The results thus demonstrate the effectiveness of the proposed constellation design tailored to the BICM-OFDM system with CAF and CNC.

We next consider the frequency-selective Rayleigh fading channel for the following two systems:

F1: BICM-OFDM without CAF (no PAPR reduction)

F2: BICM-OFDM with CAF and CNC.

The BMI values are compared in Fig. 10, where the parameters of the NENU constellations are fixed as either Mode A or C over the entire channel SNR, along with the uniform PAM as a reference. It is observed that for **F1**, the shaping gains achieved by the proposed constellations decrease compared to the results over the AWGN channel. This may be due to the fact that a single modulation scheme is applied across all subcarriers, while they experience different effective SNRs. Nevertheless, in **F2**, significant gains by the proposed shaping are still observed when compared at the target information rate. Additionally, Mode C (optimized for this system over fading channel) offers enhanced performance over Mode A.

V. SIMULATION RESULTS

We evaluate the system-level performance of the BICM-OFDM systems employing the proposed NENU constellations in the presence of CAF and CNC. As performance measures, we consider the distribution of PAPR as well as BER. For the binary channel code, we utilize the original rate-1/3 turbo code with rate-compatible puncturing [46]. The simulation setup is summarized in TABLE II. We compare the three systems:

- S1**: Conventional BICM-OFDM without PAPR reduction.
- S2**: BICM-OFDM employing CAF and CNC ($\gamma_{CR} = 1.5$).
- S3**: BICM-OFDM employing DFT precoding.

TABLE II
SIMULATION SETUP.

OFDM	1024 subcarriers
Modulation	32-PAM per dimension
Coding	Punctured turbo code
Decoding	Log-MAP (iteration: 15)
Code rate	5/6
Codeword length	30720
Spectral efficiency	8.333 bits per subcarrier
PAPR reduction	CAF ($\gamma_{CR} = 1.5$, $J = 4$) or DFT precoding
PAPR evaluation	Four-times oversampling
CNC	$K_{max} = 10$
Channel	AWGN or Rayleigh fading
Fading channel	4-path equal-power delay profile

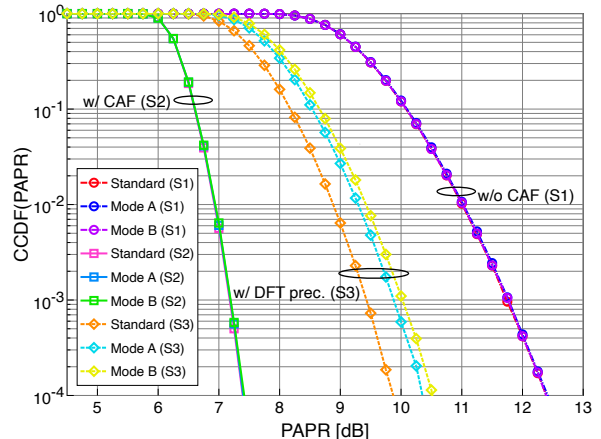


Fig. 11. Comparison of the CCDF of PAPR among the three systems: conventional OFDM without CAF, OFDM with CAF, and OFDM with DFT precoding (single-carrier). For each system, the three PAM constellations (uniform, Mode A, and Mode B) are evaluated.

Note that **S3** is equivalent to a single-carrier system with rectangular pulse shaping filter and thus its PAPR has direct dependence on the constellation [47].

For each system, we evaluate the uniform PAM, the proposed NENU constellations (parameter sets: Modes A, B, and C), and the one-dimensional NUC of ATSC 3.0. For **S3**, the conventional minimum mean square error (MMSE) detector is implemented at the receiver for the frequency-selective fading channel.

A. CCDF of PAPR

The CCDF curves of the PAPR among the three systems are compared in Fig. 11, where the three PAM constellations (uniform as well as NENU with Modes A and B) are compared.

We observe no difference among the three curves plotted for **S1** and **S2**, suggesting that each subcarrier constellation does not affect PAPR distribution for OFDM. On the other hand, in **S3**, the selection of constellations significantly affects the dynamic range of the transmit signals, indicating that the use of constellation shaping increases the PAPR as expected [48], even though it is still less than the conventional OFDM (**S1**). In contrast, from the results of **S2**, we observe that CAF effectively reduces the peak power of OFDM signals, even in the presence of constellation shaping, achieving a PAPR

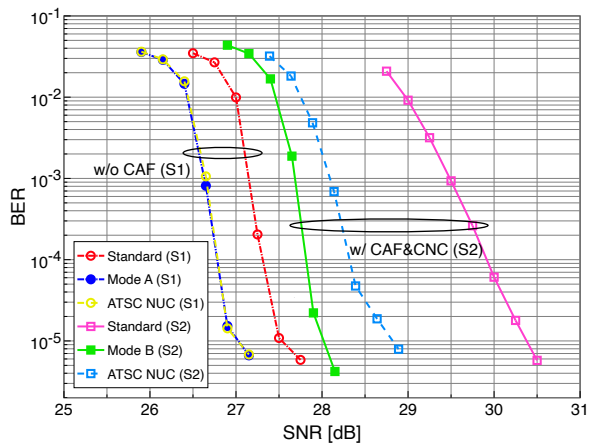


Fig. 12. BER comparison over an AWGN channel for the BICM-OFDM systems without CAF (no PAPR reduction) and with CAF/CNC employing three different PAM constellations.

reduction of 5.0 dB compared to **S1** when measured at a CCDF of 10^{-4} .

B. BER Comparison Over AWGN Channel

The BER performance over an AWGN channel for the BICM-OFDM systems with different constellations is compared in Fig. 12, evaluating either without CAF (no PAPR reduction) or with CAF and CNC. As for constellations, Modes A and B are applied to **S1** and **S2**, respectively. In addition, the uniform PAM and one-dimensional NUC adopted in ATSC 3.0 are applied to both systems. (Note that the results of **S3** are omitted as they exhibit similar performance to **S1** over the AWGN channel.) In the case of **S1**, it can be confirmed that the performance gain achieved by Mode A agrees with that estimated from the BMI values in Fig. 9. The performance is also comparable to that achieved by the one-dimensional NUC of ATSC 3.0.

On the other hand, in the case of **S2**, Mode B achieves a significant gain, yielding an improvement of approximately 2.35 dB over the uniform PAM and 0.75 dB over the NUC when evaluated at a BER of 10^{-5} . This gain, combined with the performance recovery achieved through CNC, significantly reduces the gap from **S1** (without PAPR reduction). It is noteworthy that the performance gap between **S1** with the uniform PAM and **S2** with Mode B is only 0.50 dB, while they have a significant difference in terms of PAPR. This suggests that the proposed NENU constellation together with CAF and CNC can significantly reduce PAPR without noticeable SNR penalty over the conventional BICM-OFDM system.

C. BER Comparison Over Fading Channel

Finally, we compare BER performance among the three systems **S1**, **S2**, and **S3** over a frequency-selective Rayleigh fading channel in Fig. 13. As for constellations, Modes A and C are applied to **S1** and **S2**, respectively. In addition, the uniform PAM and one-dimensional NUC adopted in ATSC 3.0 are applied to all three systems for comparison. The performance of **S2** is found effective over fading channels, achieving a gain of approximately 2.50 dB with the proposed

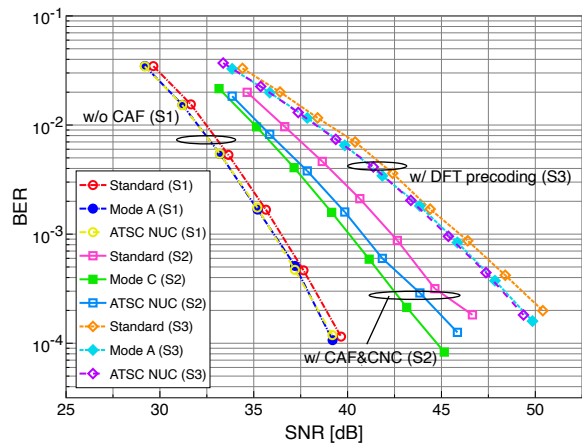


Fig. 13. BER comparison over a frequency-selective Rayleigh fading channel for the BICM-OFDM systems without CAF (no PAPR reduction), with CAF/CNC, and with DFT precoding, each employing three different PAM constellations.

NENU constellation. On the other hand, the performance of **S3** (employing an MMSE detector) is considerably inferior to that of the other OFDM-based systems. It is known that single-carrier signals experience BER degradation when suboptimal detectors, such as MMSE, are employed at the receiver [49, 50]. The results thus indicate that the performance loss associated with DFT precoding is more substantial than that caused by CAF with CNC. Consequently, for PAPR reduction in OFDM systems utilizing constellation shaping, CAF combined with CNC is superior to DFT precoding in terms of both the PAPR reduction effect and BER performance over fading channels.

VI. CONCLUSION

In this work, we developed high-capacity and low-PAPR OFDM-BICM systems based on one-dimensional NENU constellations for shaping gain along with CAF and CNC for efficient signal peak power reduction without noticeable performance degradation. As a result, the developed systems enjoy significantly lower PAPR while achieving comparable performance with the standard PAM-based BICM-OFDM system. The simulation results have demonstrated that significant performance gain can be achieved over the conventional BICM-OFDM with DFT precoding in terms of both PAPR distribution and BER. In our simulations, we have restricted our attention to the design of 32-PAM (i.e., 1024-QAM), but its extension to even higher-order constellations targeting even higher information rates is straightforward, considering the simplicity of the optimization process based on only the two distinct parameters.

REFERENCES

- [1] L. Szczecinski and A. Alvarado, Bit-interleaved coded modulation: fundamentals, analysis and design. John Wiley & Sons, 2015.
- [2] F. Steiner and G. Böcherer, "Comparison of geometric and probabilistic shaping with application to ATSC 3.0," in *Proc. ITG Conf. Systems, Commun. and Coding (SCC'17)*. VDE, 2017, pp. 1–6.
- [3] Z. Qu and I. B. Djordjevic, "On the probabilistic shaping and geometric shaping in optical communication systems," *IEEE Access*, vol. 7, pp. 21 454–21 464, 2019.
- [4] P. Schulte and G. Böcherer, "Constant composition distribution matching," *IEEE Trans. Inf. Theory*, vol. 62, no. 1, pp. 430–434, 2015.

- [5] L. Fay, L. Michael, D. Gómez-Barquero, N. Ammar, and M. W. Caldwell, "An overview of the ATSC 3.0 physical layer specification," *IEEE Trans. Broadcast.*, vol. 62, no. 1, pp. 159–171, 2016.
- [6] P. K. Singya, P. Shaik, N. Kumar, V. Bhatia, and M.-S. Alouini, "A survey on higher-order QAM constellations: Technical challenges, recent advances, and future trends," *IEEE Open J. Commun. Soc.*, vol. 2, pp. 617–655, 2021.
- [7] E. Sillekens, G. Liga, D. Lavery, P. Bayvel, and R. I. Killey, "High-cardinality geometrical constellation shaping for the nonlinear fibre channel," *IEEE J. Lightw. Tech.*, vol. 40, no. 19, pp. 6374–6387, 2022.
- [8] K. Gümüş, B. Chen, T. Bradley, and C. Okonkwo, "A simplified method for optimising geometrically shaped constellations of higher dimensionality," *arXiv preprint arXiv:2307.05179*, 2023.
- [9] B. Chen, Y. Lei, G. Liga, Z. Liang, W. Ling, X. Xue, and A. Alvarado, "Geometrically-shaped multi-dimensional modulation formats in coherent optical transmission systems," *J. Lightw. Tech.*, vol. 41, no. 3, pp. 897–910, 2022.
- [10] Advanced Television Systems Committee, *ATSC Standard: Physical Layer Protocol (A/322)*. A/322:2021, Jan. 2021.
- [11] H. Ochiai, "An analysis of band-limited communication systems from amplifier efficiency and distortion perspective," *IEEE Trans. Commun.*, vol. 61, no. 4, pp. 1460–1472, 2013.
- [12] H. Ochiai and H. Imai, "On the distribution of the peak-to-average power ratio in OFDM signals," *IEEE Trans. Commun.*, vol. 49, no. 2, pp. 282–289, Feb. 2001.
- [13] —, "Performance analysis of deliberately clipped OFDM signals," *IEEE Trans. Commun.*, vol. 50, no. 1, pp. 89–101, 2002.
- [14] H. Chen and A. M. Haimovich, "Iterative estimation and cancellation of clipping noise for OFDM signals," *IEEE Commun. Lett.*, vol. 7, no. 7, pp. 305–307, 2003.
- [15] Y. Sun and H. Ochiai, "Performance analysis and comparison of clipped and filtered OFDM systems with iterative distortion recovery techniques," *IEEE Trans. Wirel. Commun.*, vol. 20, no. 11, pp. 7389–7403, Nov. 2021.
- [16] M. Wachowiak and P. Kryszkiewicz, "Clipping noise cancellation receiver for the downlink of massive MIMO OFDM system," *IEEE Trans. Commun.*, vol. 71, no. 10, pp. 6061–6073, 2023.
- [17] E. Kurihara and H. Ochiai, "A systematic and low-complexity constellation shaping design for rate-adaptive bicom systems based on nonuniform qam," in *Proc. IEEE Consum. Commun. & Netw. Conf. (CCNC'25)*. IEEE, 2025, pp. 1–6.
- [18] H. G. Myung, J. Lim, and D. J. Goodman, "Single carrier FDMA for uplink wireless transmission," *IEEE Veh. Tech. Magaz.*, vol. 1, no. 3, pp. 30–38, 2006.
- [19] T. Koike-Akino, Y. Wang, S. C. Draper, K. Sugihara, and W. Matsumoto, "Bit-interleaved polar-coded OFDM for low-latency M2M wireless communications," in *Proc. IEEE Int. Conf. Commun. (ICC'17)*. IEEE, 2017, pp. 1–7.
- [20] B. Wiens and D. C. Lee, "Constellation design with equal-probability partition of a cropped Gaussian distribution," in *Proc. IEEE 92nd Veh. Tech. Conf. (VTC'20-F)*. IEEE, 2020, pp. 1–5.
- [21] J. J. Boutros, U. Erez, J. Van Wousterghem, G. I. Shamir, and G. Zémor, "Geometric shaping: low-density coding of Gaussian-like constellations," in *Proc. IEEE Inf. Theory W. (ITW'18)*. IEEE, 2018, pp. 1–5.
- [22] F.-W. Sun and H. C. Van Tilborg, "Approaching capacity by equiprobable signaling on the Gaussian channel," *IEEE Trans. Inf. Theory*, vol. 39, no. 5, pp. 1714–1716, 1993.
- [23] E. Kurihara and H. Ochiai, "Design of low-complexity coded modulation employing high-order QAM with systematic geometric constellation shaping," *IEEE Open J. Commun. Soc.*, vol. 5, pp. 4061–4074, 2024.
- [24] M. Yankov, S. Forchhammer, K. J. Larsen, and L. P. Christensen, "Rate-adaptive constellation shaping for near-capacity achieving turbo coded BICM," in *Proc. IEEE Int. Conf. Commun. (ICC'14)*. IEEE, 2014, pp. 2112–2117.
- [25] R. Y. Chang, S.-J. Lin, and W.-H. Chung, "Symbol and bit mapping optimization for physical-layer network coding with pulse amplitude modulation," *IEEE Trans. Wirel. Commun.*, vol. 12, no. 8, pp. 3956–3967, 2013.
- [26] L. Zhou, H. He, Y. Zhang, Y. Chen, Q. Xiao, and Z. Dong, "Enhancement of spectral efficiency and power budget in WDM-PON employing LDPC-coded probabilistic shaping pam8," *IEEE Access*, vol. 8, pp. 45 766–45 773, 2020.
- [27] M. P. Yankov, F. Da Ros, E. P. da Silva, S. Forchhammer, K. J. Larsen, L. K. Oxenløwe, M. Galili, and D. Zibar, "Constellation shaping for WDM systems using 256QAM/1024QAM with probabilistic optimization," *J. Lightw. Tech.*, vol. 34, no. 22, pp. 5146–5156, 2016.
- [28] X. Jia, Y. Li, M. Luo, C. Yang, W. Liu, X. Hong, J. Qiu, H. Guo, Z. Yang, and J. Wu, "Many-to-one mapping based truncated probabilistic shaped 64-QAM for metro transmissions enabled by polar code," *J. Lightw. Tech.*, vol. 41, no. 21, pp. 6700–6709, 2023.
- [29] Z. Cao, Y. Chen, X. Zhao, L. Zhou, and Z. Dong, "Probabilistic shaping 44QAM based on many-to-one mapping in DMT-WDM-PON," *IEEE Photon. Tech. Lett.*, vol. 32, no. 11, pp. 639–642, 2020.
- [30] Z. Li, O. Huang, A. Yan, G. Li, B. Dong, W. Shen, S. Xing, J. Shi, Z. Li, C. Shen *et al.*, "Model-free end-to-end deep learning of joint geometric and probabilistic shaping for optical fiber communication in IM/DD system," *J. Lightw. Tech.*, 2024.
- [31] A. Soleimanzade, M. A. Soleimanzade, A. Abolfathimomtaz, M. Ardakani, and H. Ebrahimzad, "Hybrid probabilistic-geometric shaped constellations to combat fiber non-linearity," in *Proc. IEEE Int. Conf. Commun. (ICC'23)*. IEEE, 2023, pp. 1946–1951.
- [32] M. Stark, F. Ait Aoudia, and J. Hoydis, "Joint learning of geometric and probabilistic constellation shaping," in *Proc. IEEE Globecom Workshops (GC Wkshps'19)*. IEEE, 2019, pp. 1–6.
- [33] R. Maneekut, S. Beppu, H. Takahashi, and T. Tsuritani, "Hybrid probabilistic and geometric shaping for 64-QAM optical fiber transmission with maximum a posteriori probability detection," in *Proc. IEEE Optoelectron. Commun. Conf. (OECC'20)*. IEEE, 2020, pp. 1–3.
- [34] H. Ochiai, "A novel trellis shaping design with both peak and average power reduction for OFDM systems," *IEEE Trans. Commun.*, vol. 52, no. 11, pp. 1916–1926, Nov. 2004.
- [35] A. Alvarado, T. Fehenberger, B. Chen, and F. M. Willems, "Achievable information rates for fiber optics: Applications and computations," *J. Lightw. Tech.*, vol. 36, no. 2, pp. 424–439, 2018.
- [36] G. Montorsi, "Design of constellation sets for multistage systems," in *Proc. IEEE Glob. Commun. Conf. (GLOBECOM'16)*. IEEE, 2016, pp. 1–6.
- [37] M. Sandell, F. Tosato, and A. Ismail, "Low complexity max-log LLR computation for nonuniform PAM constellations," *IEEE Commun. Lett.*, vol. 20, no. 5, pp. 838–841, 2016.
- [38] M. Fuentes, D. Vargas, and D. Gomez-Barquero, "Low-complexity demapping algorithm for two-dimensional non-uniform constellations," *IEEE Trans. Broadcast.*, vol. 62, no. 2, pp. 375–383, 2015.
- [39] J. Barrueco, J. Montalban, P. Angueira, C. A. Nour, and C. Douillard, "Low complexity adaptive demapper for 2-D non-uniform constellations," *IEEE Trans. Broadcast.*, vol. 65, no. 1, pp. 10–19, 2018.
- [40] H. Hong, Y. Xu, Y. Wu, Y. Huang, N. Gao, D. He, H. Li, Y. Zhang, and W. Zhang, "Enhanced nonuniform constellations for high-capacity communications with low-complexity demappers," *IEEE Trans. Broadcast.*, vol. 68, no. 3, pp. 740–752, 2022.
- [41] Y. Huang, S. Hu, S. Ma, Z. Liu, and M. Xiao, "Designing Low-PAPR waveform for OFDM-based RadCom systems," *IEEE Trans. Wirel. Commun.*, vol. 21, no. 9, pp. 6979–6993, 2022.
- [42] F. Ait Aoudia and J. Hoydis, "Waveform learning for next-generation wireless communication systems," *IEEE Trans. Commun.*, vol. 70, no. 6, pp. 3804–3817, 2022.
- [43] J. Lorca Hernando and A. G. Armada, "Frequency-modulated OFDM: A new waveform for high-mobility wireless communications," *IEEE Trans. Commun.*, vol. 71, no. 1, pp. 540–552, 2023.
- [44] Y. Qin, A. Li, Y. Lyu, X. Liao, and C. Masouros, "Symbol-level precoding for PAPR reduction in multi-user MISO-OFDM systems," *IEEE Trans. Wirel. Commun.*, vol. 23, no. 9, pp. 12 484–12 498, 2024.
- [45] C. H. Azolini Tavares, J. C. Marinello Filho, C. M. Panazio, and T. Abrão, "Input back-off optimization in OFDM systems under ideal pre-distorters," *IEEE Wirel. Commun. Lett.*, vol. 5, no. 5, pp. 464–467, 2016.
- [46] J. Li, Q. Chen, S. Gao, Z. Ma, and P. Fan, "The optimal puncturing pattern design for rate-compatible punctured turbo codes," in *Proc. 2009 Int. Conf. Wirel. Commun. & Signal Process. (WCSP'09)*, 2009, pp. 1–5.
- [47] H. Ochiai, "On instantaneous power distributions of single-carrier FDMA signals," *IEEE Wirel. Commun. Lett.*, vol. 1, no. 2, pp. 73–76, Apr. 2012.
- [48] A. Kakkavas, W. Xu, J. Luo, M. Castañeda, and J. A. Nossek, "On PAPR characteristics of DFT-s-OFDM with geometric and probabilistic constellation shaping," in *IEEE 18th Int. Works. Sign. Process. Advanc. in Wirel. Commun. (SPAWC'17)*, 2017, pp. 1–5.
- [49] A. Nasri and R. Schober, "Performance of BICM-SC and BICM-OFDM systems with diversity reception in non-Gaussian noise and interference," *IEEE Trans. Commun.*, vol. 57, no. 11, pp. 3316–3327, 2009.
- [50] A. Tajer and A. Nosratinia, "Diversity order in ISI channels with single-carrier frequency-domain equalizers," *IEEE Trans. Wirel. Commun.*, vol. 9, no. 3, pp. 1022–1032, 2010.